

2-D and 3-D Interactions in Random Sequential Adsorption of Charged Particles

Matthew R. Oberholzer,* Jim M. Stankovich,† Steven L. Carnie,† Derek Y. C. Chan,† and Abraham M. Lenhoff*¹

†*Department of Mathematics and Statistics, University of Melbourne, Parkville 3052, Australia; *Center for Molecular and Engineering Thermodynamics, Department of Chemical Engineering, University of Delaware, Newark, Delaware 19716*

Received March 31, 1997; accepted July 24, 1997

We explore the influence of electrolyte concentration on the adsorption of charged spheres using modeling techniques based on random sequential adsorption (RSA). We present a parametric study of the effects of double layer interactions between the charged particles and between the particle and the substrate on the jamming limit using a two-dimensional RSA simulation similar to that of Z. Adamczyk *et al.* (1990, *J. Colloid Interface Sci.* 140, 123) along with a simple method of estimating jamming limit coverages. In addition, we present a more realistic RSA algorithm that includes explicit energetic interaction in three dimensions, that is, particle–particle and particle–surface interactions during the approach of a particle to the substrate. The calculation of interaction energies in the 3-D RSA model is achieved with the aid of a three-body superposition approximation. The 3-D RSA model differs from the 2-D model in that the extent of coverage is controlled by kinetic rather than energetic considerations. Results of both models capture the experimentally observed trend of increased surface coverage with increased electrolyte concentration, and both models require the value of a key model parameter to be specified for a quantitative match to experimental data. However, the 3-D model more effectively captures the governing physics, and the parameter in this case takes on more meaningful values than for the 2-D model. © 1997 Academic Press

Key Words: colloidal electrostatic interactions; superposition approximation; simulation.

1. INTRODUCTION

The extent of physisorption at interfaces is usually characterized in terms of an adsorption isotherm in which the adsorbate concentration at the interface is related to that in the bulk solution. At low coverages the adsorbate molecules at the interface are sufficiently widely separated that the isotherm reflects simply the interactions between isolated adsorbate molecules and the interface. At higher coverages, however, the situation becomes more complicated, even when adsorption does not proceed beyond a monolayer.

Here, increasing coverage both reduces the amount of interfacial area available for adsorption and increases the proximity of adsorbate molecules to one another, thereby making this situation more complex than the low coverage limit. Since high coverages are also of technological interest in view of the more efficient use of adsorbent capacity, the development of effective and realistic approaches for modeling this behavior is of great practical importance.

The most widely used basis for modeling adsorption is that due to Langmuir, who considered adsorption to take place at individual, independent sites, each able to accommodate one adsorbate molecule. Consideration of reversible mass action kinetics then led to the well-known hyperbolic isotherm. Experimental data from a very wide variety of systems have been fitted to the Langmuir form despite clear deviations, in many cases, from the assumptions inherent in the Langmuir model. As a result, the parameters obtained in these studies have had only descriptive value in the curve-fitting sense, and have not provided predictive mechanistic capabilities. Deviations of several kinds are possible: (i) absence of clearly defined adsorption sites; (ii) deviations from microscopic reversibility of adsorption, typically in the form of irreversibility; (iii) interactions among neighboring adsorbate molecules.

Different combinations of these discrepancies are observed in different systems, and the development of more realistic models of adsorption at high coverages must address these in each case. For example, in adsorption of small molecules, such as gases on graphite, reversible adsorption occurs on reasonably well-defined sites, but interactions among adsorbate molecules are important at high coverages (2, 3). For the adsorption of colloidal particles, on the other hand, the characteristic particle dimensions are large enough to make identification of sites on the adsorbent interface impossible; instead, the interface is more appropriately treated as a continuum. Furthermore, depending on the nature of the adsorbent, the adsorbate and the solvent, a range of degrees of reversibility is possible, as reflected, for instance, in the wide range of behavior reported in the protein adsorption literature (4). In general, the dependence of dispersion inter-

¹ To whom correspondence should be addressed. Fax: +1-302-831-4466. E-mail: lenhoff@che.udel.edu.

actions on particle size increases the likelihood of irreversible adsorption with increasing particle size since a typical adsorption energy per particle can be much greater than the thermal energy. Irreversible adsorption can not be fully described by purely thermodynamic considerations, and kinetic processes must be incorporated explicitly. Finally, for colloidal particles both steric and energetic interactions may be important. The steric interactions lead to excluded-area effects that are qualitatively equivalent to the site saturation feature of the Langmuir model, but if the adsorbed particles are considered to be a fluid phase, the isotherm is much “softer” than the Langmuir form (5). In the presence of energetic interactions, even more complex coverage dependence results.

Our interest is in adsorption of charged colloidal particles and particularly in the increasing effect of interactions among adsorbate molecules at high coverages. Even under the assumption of fully reversible adsorption on well-defined sites, adsorption of colloidal particles differs from that of small molecules in that the latter are usually considered to interact via attractive dispersion interactions, while the former can also display electrostatic repulsion. However, as noted above, the adsorbent in adsorption of colloidal particles is more realistically considered to be a continuum than an array of sites, and under these circumstances there also enters into any modeling effort an enormous configurational problem as a result of the lateral degrees of freedom available to adsorbate particles.

A variety of models is available for describing adsorbate properties under these circumstances, but the picture is not yet complete. Two-dimensional gas models (2, 6) are most often used for describing small, mobile adsorbates, such as surfactants at fluid–fluid interfaces, but they have also been applied to adsorption of more massive particles such as proteins (5). However, such approaches are less suitable in the presence of long-range interactions, and under these circumstances two-dimensional Brownian dynamics simulations (7, 8) are more appropriate, with the particle dynamics in the plane of the interface serving to provide configurational exploration. The extent of adsorption is related to interparticle and particle–surface energetics by equating the chemical potential of adsorbed particles to that of those in solution. Three-dimensional Brownian dynamics simulations can capture the adsorption process even more explicitly (9), but such simulations are very expensive computationally, and they rarely offer simplified limiting expressions for routine use. Reducing the computational effort requires some idealization to reduce the configurational complexity. One example is to assume the adsorbate molecules to self-assemble into an ordered array (10) and to interact via repulsive electrostatic and attractive dispersion forces. Although there is experimental evidence to support the ordering assumption in the case of protein adsorption, the model can also be

considered to provide a semiquantitative indication of the effect of increasing coverage even when ordering is absent.

An alternative limiting assumption to that of perfect order is that of total randomness, the best known implementation of which is the random sequential adsorption (RSA) model (11, 12). Here adsorbed particles are assumed to be frozen in position irreversibly, and attempts are made to place additional particles on the surface at random; placement is deemed successful if there is no overlap with previously placed particles. The RSA model captures some of the key features of colloidal adsorption, notably the irreversible and immobilizing adsorption expected of large particles, but it is quite different to other models in several respects. First, it is a kinetic model incapable of describing thermodynamic equilibrium (although the kinetic behavior of this model at low coverage is similar to that of equilibrium adsorption (13, 14)): adsorption continues until no more particles can be placed, a situation known as the jamming limit (approximately 54.7% of the adsorbent surface area for monodisperse spheres). Second, it accounts only for steric effects, and omits all consideration of energetics. The first of these differences is not a shortcoming in that it reflects the largely irreversible nature of colloidal adsorption, but the omission of energetic interactions limits the applicability of the RSA model to real systems. Nonetheless, the conceptual simplicity of the model and the compact form of the result makes it an attractive basis for development of more realistic descriptions.

In this work we present a modified RSA model in which interparticle energetics are accounted for in the form of electrostatic repulsion: for an attempt at placing an additional particle to be successful, there must be not just an absence of overlap, but in addition the cumulative energy of repulsion from previously adsorbed particles must not exceed a certain threshold. This algorithm is similar to one previously presented by Adamczyk *et al.* (1), but we go beyond that work in several different respects. First, we present more extensive results showing the jamming limits predicted under different conditions, including a very simple approximate method for estimating them. These jamming limits are, of course, lower than the conventional RSA value in general. The extent of the reduction depends on key parameters characterizing the interparticle interactions, and we present relationships for estimating these efficiently and accurately. This fairly simple, computationally efficient model appears to be capable of describing adsorption extents observed experimentally, but only by virtue of an adjustable model parameter, the value of which cannot be predicted a priori. The reason for this deficiency is that the model does not fully capture the physics of the problem, and we remedy this using another novel RSA model that considers events during the approach of a particle to the surface, and not just the energetics of particles already at the surface.

The remainder of the paper is organized as follows. First,

a superposition approximation used to simplify the three-body (particle–particle–surface) interaction calculations is presented. The methods for calculating interaction energies between particles and between particles and the surface are then given. Next, the details of the two RSA simulations are discussed, with emphasis on the physical events each model is designed to capture. Finally, the simulation results for both simulations are presented, and general trends and comparison to experiment are discussed, along with the analysis that leads to a simple method of estimating surface coverage.

2. ENERGETICS

In order to study the adsorption behavior of charged particles, interaction energies between two particles and between a particle and the surface must be known as accurately as possible. In this section we present the pair potentials used to calculate particle–particle and particle–surface interaction energies, along with methods used to calculate potential parameters. Proper calculation of the interaction energy between particles near the adsorption surface is quite complicated, and full exploration of the relevant parameter space is beyond the scope of the present work. Our focus here is on the range of conditions covered by the experimental system of Johnson and Lenhoff (15), who studied the adsorption of spherical amidine polystyrene latex particles onto a mica surface using atomic force microscopy (AFM); these data also provide a basis for testing the validity of the RSA calculations. We present a three-body superposition approximation that simplifies the task of calculating the interactions for this particular system. The results of this calculation show that the energetics are sufficiently accurately described using pair interactions, which can in turn be parameterized using previously developed analytic approximations. The applicability of these approximations to systems other than the latex–mica one will have to be assessed using the methods presented here, but in general they are most suitable for larger and more strongly repulsive particles.

2.1. A Superposition Approximation for a Three-Body System

The accurate calculation of adsorption behavior at high surface coverages requires particle–particle and particle–surface interactions to be accounted for simultaneously. Suppose we have two particles of radius a at a distance H from the surface and a distance R (measured from center to center) from one another. The other important length scale is the Debye length κ^{-1} . We are guided by the latex–mica experiments (15) in which the observed particle–particle separations R range from 150 to 250 nm (see Table 1). These produce values of the scaled separation κd (measured particle surface to particle surface, $d = R - 2a$) in the range 4.4 to 19. Numerical calculations show the superposition

TABLE 1
Pairwise Energies for the Amidine Polystyrene–Mica System

NaCl conc. (mM)	0.1	1	5	20
κa	1.9	6.0	13	27
θ_{\max} , exp. (%)	19.5	27.5	45.5	49
U_{ps}^{dl} (kT) ^a	−5941	−2796	−1369	−603
U_{ps}^{vdw} (kT) ^a	−370	−370	−370	−370
R^* (θ_{\max}) (nm)	250	211	164	158
κd^*	4.4	9.9	11	19
U_{pp}^{dl} (kT) ^b	5.3	0.016	0.0039	5.3×10^{-7}
U_{pp}^{vdw} (kT) ^b	−0.00092	−0.0030	−0.022	−0.031

^a Latex–mica energies U_{ps} calculated at $H = 0.1$ nm.

^b Latex–latex energies U_{pp} calculated at $R = R^*$ (defined in Eq. [13]).

approximation to be very accurate for such (scaled) separations (16). This suggests that some sort of superposition argument may also be applicable to two adsorbed particles. We will need to superimpose two solutions for the potential around a single adsorbed particle.

We have two particles a distance H from the mica surface (about which we make no assumptions yet) and a large distance R from one another (at which the standard superposition approximation is accurate). From now on we use dimensionless potentials (scaled by kT/e), positions and separations (scaled by a) and forces (scaled by $\epsilon \epsilon_0 (kT/e)^2$), where ϵ is the dielectric constant, ϵ_0 is the permittivity of free space, and e the electronic charge. Let

- $\psi_s(\mathbf{x})$ denote the potential (as a function of position) around the planar surface in isolation
- $\psi_{sp_i}(\mathbf{x})$ denote the potential around the surface and the i th particle in isolation (the potential when the other particle is at infinite separation R ; $i = 1, 2$)
- $\delta_i(\mathbf{x}) = \psi_{sp_i}(\mathbf{x}) - \psi_s(\mathbf{x})$ be the perturbation to the isolated planar surface potential caused by the presence of particle i ($i = 1, 2$),

where the subscript s denotes the (planar) adsorption surface and p denotes the spherical particle. Then take our superposition approximation ψ_{sup} to the potential to be

$$\psi_{\text{sup}} \equiv \psi_{sp_1} + \psi_{sp_2} - \psi_s = \psi_s + \delta_1 + \delta_2. \quad [1]$$

That is, superimpose the perturbations δ_1 and δ_2 caused by the two particles on the potential ψ_s . ψ_{sup} satisfies the boundary condition on the surface. It is accurate around particle 1, where δ_2 is very small (and vice versa around particle 2). As in the case of the standard superposition approximation, we are most interested in the accuracy of ψ_{sup} on the midplane between the particles, where we will integrate it to calculate the repulsive force. On this plane, where δ_1 and δ_2 are both small, we can use the fact that, for $\delta \ll \psi$,

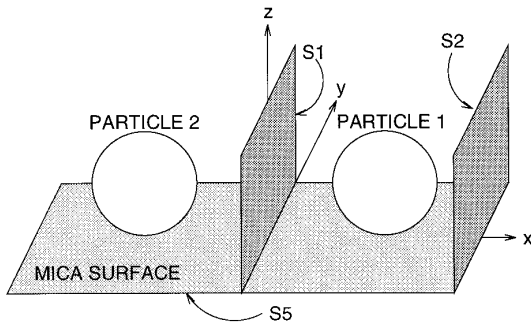


FIG. 1. Schematic for the calculation of the force between two spheres in the vicinity of a mica surface.

$$\sinh(\psi + \delta) = \sinh \psi + \delta \cosh \psi + O(\delta^2) \quad [2]$$

to show that ψ_{sup} approximately satisfies the Poisson–Boltzmann equation:

$$\begin{aligned} \nabla^2 \psi_{\text{sup}} &= \nabla^2 \psi_{\text{sp}_1} + \nabla^2 \psi_{\text{sp}_2} - \nabla^2 \psi_s \\ &= \sinh \psi_{\text{sp}_1} + \sinh \psi_{\text{sp}_2} - \sinh \psi_s \\ &= \sinh \psi_s + (\sinh \psi_{\text{sp}_1} - \sinh \psi_s) \\ &\quad + (\sinh \psi_{\text{sp}_2} - \sinh \psi_s) \\ &\simeq \sinh \psi_s + (\psi_{\text{sp}_1} - \psi_s) \cosh \psi_s \\ &\quad + (\psi_{\text{sp}_2} - \psi_s) \cosh \psi_s + O(\delta_1^2 + \delta_2^2) \\ &\simeq \sinh \psi_s + (\delta_1 + \delta_2) \cosh \psi_s + O(\delta_1^2 + \delta_2^2) \\ &\simeq \sinh \psi_{\text{sup}} + O(\delta_1^2 + \delta_2^2). \end{aligned} \quad [3]$$

We wish to know whether the work required to bring two adsorbed particles together differs significantly from the work required to bring two isolated particles together. In both cases the work can be calculated by integrating the component of the repulsive force in the direction of movement, so, for the purposes of our comparison, it suffices to compare these forces.

It is important to note that, because we are superposing two perturbations, it is necessary to specify the boundary conditions on the particles and the surface; otherwise we cannot calculate the perturbations δ_1 , δ_2 at the small separations typical of adsorbed particles. Again we are guided by the experimental system and take the particles to have constant surface charge density and the surface to have constant surface potential. The actual values assigned to these parameters are discussed later.

Consider the surface and two adsorbed particles shown in Fig. 1. The surface lies in the plane $z = 0$, and the centers of particles 1 and 2 lie above the x -axis with the plane $x = 0$ the midplane between them. The x -component of the force

(call it f) exerted on particle 1 by the surface and particle 2 is equal to

$$\mathbf{i} \cdot \int_{\Omega} \mathbf{T} \cdot \mathbf{n} dS, \quad [4]$$

where \mathbf{i} is the unit vector in the x -direction, Ω is a surface enclosing particle 1 with outward unit normal \mathbf{n} and

$$\mathbf{T} = \nabla \psi \nabla \psi - \left[\frac{1}{2} |\nabla \psi|^2 + (\cosh \psi - 1) \right] \mathbf{I} \quad [5]$$

is the stress tensor (\mathbf{I} is the unit tensor). Choose Ω to be a box with sides $x = 0$ ($S1$), $x = \xi$ ($S2$), $y = \pm \eta$ ($S3$ and $S4$), $z = 0$ ($S5$) and $z = \zeta$ ($S6$), and let ξ , η , and ζ approach infinity. Then the contributions to f from the sides $S3$, $S4$, $S5$ and $S6$ vanish. (The contribution from $S5$ vanishes because $(\partial \psi / \partial x) = 0$ on the mica surface at $z = 0$ as the surface is assumed to be at constant potential.) We are left with

$$\begin{aligned} f &= \int_{S1} \left[(\cosh \psi - 1) + \frac{1}{2} \left(\frac{\partial \psi}{\partial y} \right)^2 + \frac{1}{2} \left(\frac{\partial \psi}{\partial z} \right)^2 \right] dS \\ &\quad - \int_{S2} \left[(\cosh \psi - 1) + \frac{1}{2} \left(\frac{\partial \psi}{\partial z} \right)^2 \right] dS. \end{aligned} \quad [6]$$

Now we can use our superposition approximation on $S1$ to write $\psi = \psi_s + 2\delta_1$, where ψ_s and δ_1 are as defined above. On $S2$, $\psi = \psi_s$. Substituting into [6], the $\cosh \psi_s$ and $(\partial \psi_s / \partial z)^2$ terms cancel, and we are left with

$$\begin{aligned} f &= 2 \int_{y=0}^{\infty} \int_{z=0}^{\infty} \left\{ 2 \cosh \psi_s \sinh^2 \delta_1 + \sinh \psi_s \sinh(2\delta_1) \right. \\ &\quad \left. + 2 \left[\frac{\partial \psi_s}{\partial z} \frac{\partial \delta_1}{\partial z} + \left(\frac{\partial \delta_1}{\partial z} \right)^2 + \left(\frac{\partial \delta_1}{\partial y} \right)^2 \right] \right\} dz dy, \end{aligned} \quad [7]$$

where we have to evaluate δ_1 on $S1$.

Equation [7] was solved using the code described in (17), which calculates the interaction between a spherical particle and flat surface. Representative values for the physical properties of the latex–mica system (see Section 2.2) were used in this calculation. The repulsive force $f(R, H)$ between two latex particles at a fixed distance R from one another hardly changes as they approach the mica surface (as H decreases from ∞ to 0.1 nm). Figure 2 shows $f(R, \infty)$ (the standard superposition approximation) and $f(R, 1 \text{ nm})$ for latex particles in 0.1 mM electrolyte solution. The Debye length for this electrolyte concentration is approximately 30 nm and $f(R, 10 \text{ nm})$ is indistinguishable from $f(R, 1 \text{ nm})$ when plotted—we can expect $f(R, 0.1 \text{ nm})$ to have the same form. (The numerical code becomes increasingly difficult

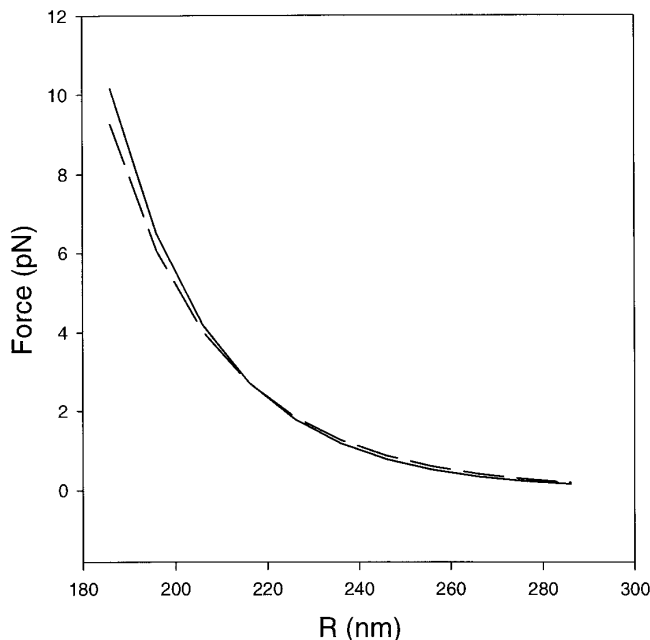


FIG. 2. The lateral repulsive force as a function of the separation distance R between two spheres at $H = 1$ nm (—) compared to the force between two spheres at $H = \infty$ (---). The electrolyte concentration is 0.1 mM, the charge on the latex is 27.4 mC/m², and the mica potential is -100 mV.

to apply as H decreases.) At the higher experimental salt concentrations, $f(R, H)$ changes even less as H decreases.

The insignificant effect of the strongly charged mica surface seems reasonable when one considers that the particles are much larger than a Debye length in diameter. As a result the surface potential changes only on a small section of the particle close to the mica—the remainder of the particle is not “aware” of the mica. The significance of this calculation is that, for lateral separations typical of the experiments, it is sufficient to approximate particle–particle interactions as if they were unaffected by the surface. This conclusion would not necessarily be valid for smaller values of κa .

2.2. Pairwise Interaction Energies

The particle–particle interaction energies can be well described with the (standard) superposition approximation for the separations relevant here. In addition, they are required as input into the RSA models to be described in the next section, so an analytic representation is highly desirable. For this purpose, we use the superposition of the outer solution found by Chew and Sen (18), which is correct to $O(1/\kappa a)^2$ (see Appendix, Eq. [24]).

This gives the dimensionless electrostatic energy U_{pp}^{dl} between two identical spherical particles of radius a , at a cen-

ter-to-center separation distance R , as an equation of Yukawa form,

$$U_{pp}^{dl}(r) = \frac{B_{pp}}{r} e^{-\kappa a(r-2)}, \quad [8]$$

where $r = R/a$, U_{pp}^{dl} is scaled by kT , and the dimensionless Yukawa coefficient for particle–particle interactions is given by

$$B_{pp} = \left(\frac{4\pi kT \epsilon \epsilon_0 a}{e^2} \right) \left(4\gamma + \frac{2}{\kappa a} \gamma^3 \right)^2. \quad [9]$$

The quantity γ is given by

$$\gamma = \tanh\left(\frac{\psi_p}{4}\right),$$

where the relation between the surface charge density, σ_p , and the dimensionless surface potential of the particle, ψ_p , is found from the corresponding inner solution (Eq. [26]), again correct to $O(1/(\kappa a)^2)$

$$\frac{\sigma_p}{\epsilon \epsilon_0 \kappa (kT/e)} = 2 \sinh \frac{\psi_p}{2} + \frac{4}{\kappa a} \tanh \frac{\psi_p}{4}. \quad [10]$$

Because they arise from expansions in $1/\kappa a$, these expressions are valid only for large κa , but they are certainly accurate enough for the values in the experimental system. For example, Eq. [10] is accurate to within 5% for all values of ψ_s when $\kappa a > 0.5$.

To calculate van der Waals interactions, Hamaker’s results were used:

$$U_{pp}^{vdw}(r) = -\frac{A_{131}}{6kT} \left[\frac{2}{r^2 - 4} + \frac{2}{r^2} + \ln\left(1 - \frac{4}{r^2}\right) \right] \quad [11]$$

$$U_{ps}^{vdw}(h) = -\frac{A_{132}}{6kT} \left[\frac{1}{h} + \frac{1}{h+2} + \ln\left(\frac{h}{h+2}\right) \right]. \quad [12]$$

Here, the dimensionless distance between the surface of the particle and the planar surface is $h = H/a$. The Hamaker constant A_{131} reflects dispersion interactions between two particles, 1, through the solution, 3. A_{132} is the Hamaker constant for the particle interacting with the surface, 2, through the solution.

We show later how these pair potential functions are used in RSA simulations, and compare simulation results to those obtained experimentally. Our present interest, though, is in the relative magnitudes of the interaction energies for the amidine polystyrene latex–mica system (15). Table 1 shows characteristic values of the interaction energies as a function

of salt concentration, taking the surface charge density of the latex particles² to be 27.4 mC/m² and the surface potential of the mica to be -100 mV. The particle radius was fixed at 58 nm. The Hamaker constants for this system were assumed to be $A_{132} = 1.6 \times 10^{-20}$ J, and $A_{131} = 0.95 \times 10^{-20}$ J (20). This means that adsorption is driven by both van der Waals and double layer forces since the particles and the surface are oppositely charged.

The interaction energies between latex particles shown in Table 1 were calculated far from the surface (as justified in Section 2.1) at an interparticle spacing $R = R^*$ based on hexagonal packing:

$$R^* = a \sqrt{\frac{2\pi}{\theta_{\max}\sqrt{3}}}. \quad [13]$$

Here, θ_{\max} is the experimental jamming limit fractional coverage (15). Particles in those experiments adsorbed in fairly irregular patterns (particularly at higher salt concentrations), so that R^* represents an average particle spacing. Nevertheless, the large values of κd^* ($=\kappa(R^* - 2a)$) mean that at most separations of interest the double layer interaction energy U_{pp}^{dl} is accurately given by the superposition approximation (see the Appendix).³ The interaction energies U_{pp}^{dl} and U_{pp}^{vdw} are plotted as a function of separation R in Fig. 3. At the separations of interest (in the tens or hundreds of nanometers), the van der Waals attraction is negligible.

Latex-mica energies were calculated at a separation distance $H = 0.1$ nm because U_{ps}^{vdw} diverges as $H \rightarrow 0$. U_{ps}^{dl} was calculated using the nonlinear Deryaguin construction, which is fairly accurate in this situation.⁴ The case of mixed boundary conditions employed here (constant charge on the latex and constant potential on the mica) was calculated as described in (22). The double layer energy U_{ps}^{dl} remains finite as $H \rightarrow 0$. As seen in Table 1, the double layer interaction dominates over the κa range of interest (U_{ps}^{vdw} and U_{ps}^{dl} are roughly equal at $\kappa a \approx 40$). In addition, the double layer repulsion U_{pp}^{dl} is much weaker than the double layer attraction U_{ps}^{dl} exerted by the mica surface.

² The surface charge density of the latex particles was calculated using the theory of O'Brien and White (19) from the mean electrophoretic mobility as measured by the manufacturer.

³ Some care must be exercised with superposition in the 0.1 mM case for $R < R^*$. Here the error in the superposition approximation is greater than 10% when $\kappa d^* < 3$. However, the experimental results (15) suggest that the particles are roughly uniformly spaced in this case, so the problem should not be too great.

⁴ The Deryaguin approximation was compared with a full numerical calculation (as described in (17)) for H down to 0.6 nm (the numerical calculation becomes cumbersome at very small separations). A similar situation is shown in Fig. 15b of (21) (squares); in our case, reduction in accuracy when $\kappa a < 10$ is offset by improvements in the Deryaguin approximation at higher potentials and when the force is integrated.

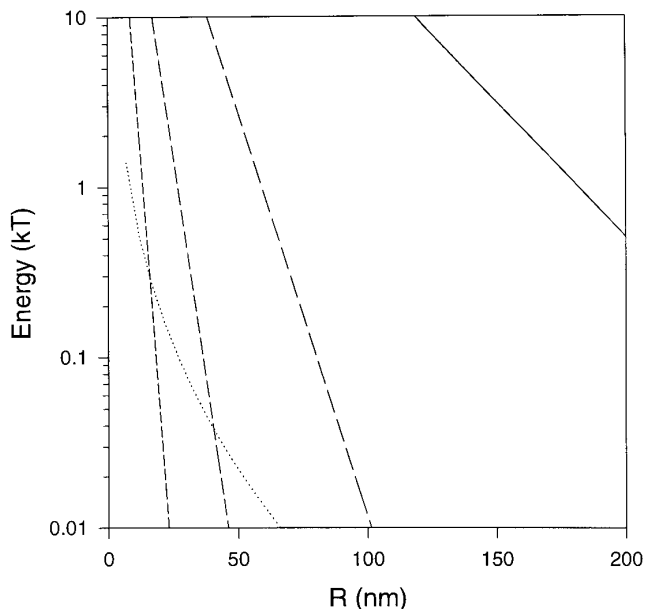


FIG. 3. U_{pp} for the amidine polystyrene latex-mica system of Johnson and Lenhoff (15) plotted as a function of separation for several ionic strengths: 0.1 mM (—); 1 mM (---); 5 mM (- - -); 20 mM (···). The absolute value of the van der Waals energy, $|U_{pp}^{vdw}|$, is also plotted (···).

The conclusion to be drawn from this analysis is that the adsorption is driven overwhelmingly by attractive double layer forces, not van der Waals forces. The attraction is so large as to make the adsorption irreversible. The observed adsorption behavior cannot be characterized by equilibrium isotherms, which would show monolayer coverage at all salt concentrations since the latex-latex interactions are so weak compared to latex-mica interactions. All these features lead one to the use of nonequilibrium adsorption models.

3. SIMULATION METHODS

Two separate RSA simulations were developed to probe the effect of particle-particle and particle-surface electrostatic interactions on the adsorption of colloidal particles. The variation of fractional coverage with salt concentration and other parameters was of primary interest. The first of the models, denoted 2-D RSA, takes into account only lateral interactions between particles on the surface; this model is similar to that of Adamczyk *et al.* (1). Although particle-surface interactions are not directly included, it is assumed, as in hard-disk RSA, that the particle-surface interaction is strong enough to attract the particles to the surface and to keep them there. In the second model, referred to as 3-D RSA, the interaction between the adsorbing particle and the surface is explicitly considered through an equation similar to Eq. [8], valid for large κa and separations large enough for superposition to apply. Here, the net attraction to the

surface depends not just upon the distance between the particle and the surface, but upon the local surface coverage as well.

3.1. 2-D RSA

The algorithm for 2-D RSA with lateral interactions is an extension of the standard hard-disk RSA model. An adsorption site for a test particle of radius a is chosen at random from a square plane of side L . In the conventional RSA algorithm, if placement of the test particle at the site would lead to overlap with particles already placed (i.e., $r < 2$), the site is abandoned and a new site is chosen at random. The 2-D RSA algorithm presented here adds an additional condition, in which the placement of the test particle is subject to energetic requirements if no overlap occurs. The energy of interaction U_{lat} between the test particle and those previously placed particles in the vicinity of the test particle is calculated assuming pairwise additivity of two-body interactions using Eq. [8],

$$U_{\text{lat}} = \sum_{\substack{j \\ r_j \leq r_c}} U_{\text{pp}}(r_j) = B_{\text{pp}} \sum_{\substack{j \\ r_j \leq r_c}} \frac{e^{-\kappa a(r_j-2)}}{r_j}, \quad [14]$$

where r_c is a cutoff radius, chosen such that $U_{\text{pp}}(r_c) = 0.01$. Van der Waals interactions are neglected in view of their small contribution (Table 1). By contrast, the particle–surface interactions dominate the particle–particle interactions included in Eq. [14] under most conditions and can be regarded as a constant background that does not affect the adsorption process. Periodic boundary conditions are used in calculating the summation in Eq. [14]. If the energy of interaction is greater than a preselected critical energy, U_c (scaled by kT), the placement of the particle is rejected. If $U_{\text{lat}} \leq U_c$, the placement is accepted. Coordinates for the placement of a new test particle are then randomly chosen, and the process is repeated. The fraction of the total area covered by particles, θ_{max} , is calculated at the end of the simulation as $\theta_{\text{max}} = N_t \pi (a/L)^2$, where N_t is the total number of successfully adsorbed particles.

The original algorithm of Adamczyk *et al.* (1) included a similar adsorption test based on lateral repulsion. Although additivity of pair interactions was incorporated into subsequent work (23, 24), in the original work only the interaction between a (potentially) adsorbed particle and its nearest neighbor was calculated, and this interaction was estimated to be one-half of that between the two particles in isolation. (Recall that for typical parameters in our work, we showed that this interaction is unchanged by the presence of the mica surface.) As we have done, the two-sphere interaction was calculated using the superposition approximation (Eq. [8]), though without including the $O(1/\kappa a)$ term. Note that the presence of the attractive surface in the model of (1) is

incorporated by halving the repulsive energy—that model does not seem to allow for the fact that an adsorbed particle with no neighbors is in a lower energy state than a particle in bulk solution. The authors also use a probabilistic acceptance criterion, which, given sufficient time, could allow energetically unfavorable placement of particles on the surface.

The description of adsorption physics in both our model and that of Adamczyk *et al.* (1) is greatly simplified. The energy change, U_{ads} , in bringing one particle from the bulk solution to the bare surface is favorable, so $U_{\text{ads}} < 0$. However, the energy of placing that particle on the surface in the presence of another particle already at the surface at a distance r away will be less favorable by an amount approximately equal to $U_{\text{pp}}(r)$. Placement of a particle in the vicinity of other particles will be less favorable by approximately U_{lat} . One simple interpretation of our algorithm is that the critical energy, U_c , reflects the maximum allowable energy penalty for successful adsorption. Thus, when the sum of the unfavorable particle–particle repulsions is greater than the favorable particle–surface attraction, placement of the particle is rejected. However, because U_c is usually not known a priori and varies for the different particles placed on the surface, it is used here as an adjustable parameter.

3.2. 3-D RSA

Only lateral interactions between particles on the surface are considered in the 2-D RSA model; therefore, the extent of adsorption is governed by particle–particle repulsion. The actual adsorption process is likely to be governed not just by energetics of the adsorbed configuration, but also by the process by which this configuration is reached. This requires direct incorporation of the particle–surface pair potential to yield a more realistic description of the adsorption physics. Consider a free particle at a dimensionless height h above the mica surface, onto which a number of particles have already adsorbed. The repulsion exerted by the adsorbed particles combined with the attraction exerted by the surface will produce an interaction energy profile $U(h)$ like that shown schematically in Fig. 4a. This profile is drawn assuming that neither electrostatic interaction nor Brownian motion causes a shift in the lateral position of the free particle as it travels toward the surface. The critical feature of the $U(h)$ profile is the presence of the energy barrier U^* at a distance $h = h^*$ above the surface. This feature represents a kinetic barrier to adsorption, distinct from the static energetic considerations in 2-D RSA. Early in the adsorption process, when there are few adsorbed particles, the energy barrier U^* will be too small to prevent adsorption: the particle will continue on to the primary minimum. When more particles have adsorbed, however, U^* may be much larger than kT , and the particle will not be able to reach the surface and adsorb. Thus with the 3-D model, the barrier to adsorption does not necessarily occur at the surface, and no estimate of U_{ads} is necessary.

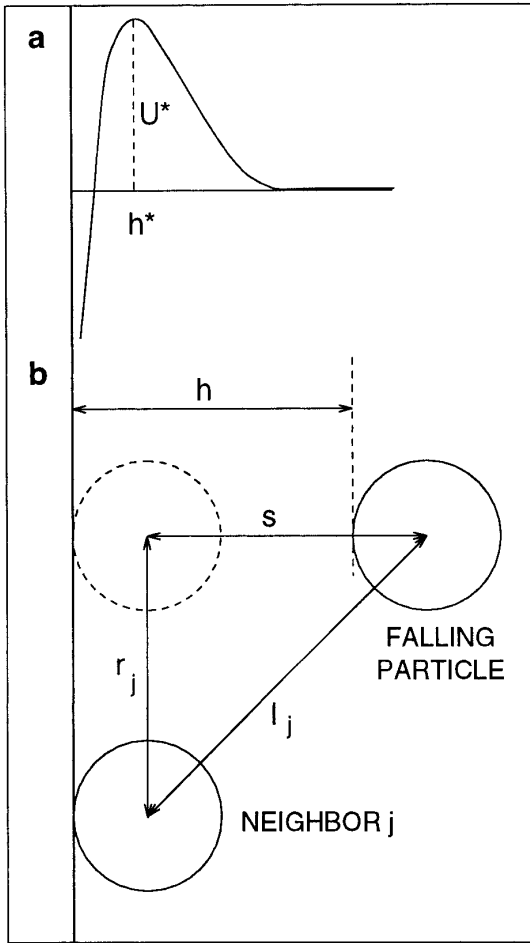


FIG. 4. (a) Schematic energy profile for a particle approaching the surface in 3-D RSA. (b) Schematic of dimensionless length scales used in 3-D RSA calculations. Note that $s = h$.

The 3-D RSA simulation requires a substantial departure from standard RSA algorithms. Coordinates in the x, y plane are chosen at random and checked so as to avoid overlap with previously placed particles. To determine whether a particular particle adsorbs during the RSA algorithm, the size of the barrier in the energy profile, U^* , must be estimated. This estimate depends upon the magnitudes of all interactions present. For the latex–mica system, for example, the calculations of Table 1 show that van der Waals interactions do not make a significant contribution to the energy. In addition, we have shown that at the separations of interest, the superposition approximation is accurate for particle–particle electrostatic interactions for both adsorbed and free particles. Furthermore, a repulsive energy barrier could arise only at a height h^* where the neighboring adsorbed particles are closer to the adsorbing particle than the strongly attractive surface. Thus the superposition approximation must also be valid for particle–surface interactions at the heights h^* of interest.

Under these circumstances, the electrostatic attraction between a particle and the adsorption surface is given in dimensionless form by

$$U_{ps}^{dl}(h) = B_{ps} e^{-\kappa ah}. \quad [15]$$

Here, the dimensionless coefficient for the particle–surface interaction is

$$B_{ps} = \left(\frac{4\pi kT\epsilon\epsilon_0 a}{e^2} \right) \left(4\gamma + \frac{2}{\kappa a} \gamma^3 \right) \left(4 \tanh \left(\frac{\psi_0}{4} \right) \right), \quad [16]$$

where ψ_0 is the dimensionless potential of the adsorption surface and γ is the same as in Eq. [9]. As before, Eqs. [15] and [16] are strictly valid only for $\kappa a \gg 1$ but are of sufficient accuracy for the present purpose.

Using the length scales defined in Fig. 4b (and noting that $s = h$ in the figure), the double layer interaction energy $U(h)$ between an adsorbing particle and its surroundings is

$$U(h) = B_{pp} \sum_j \frac{e^{-\kappa a(l_j - 2)}}{l_j} + B_{ps} e^{-\kappa ah}, \quad [17]$$

where $l_j = \sqrt{r_j^2 + h^2}$ is the center-to-center distance between the adsorbing particle and its j th adsorbed neighbor. The algorithm was implemented by using Newton-Raphson iteration to search for a maximum, U^* . An initial guess $h_0 = \min_j \{r_j - 2\}$ was used. At this low h value the mica surface will dominate and ensure that the scaled vertical force $-U'(h)$ is negative (attractive). If $U(h)$ is ever positive, the convex form of $U(h)$ will yield rapid convergence. If the neighbors are sufficiently far away, however, $U(h)$ will be negative for all h and may not have a maximum. Thus it is assumed that the particle adsorbs if the iteration does not converge. To speed the calculations, only the interactions with the six nearest neighbors were considered.

Once U^* is estimated, the placement attempt becomes subject to energetic requirements. U^* is compared to a preselected maximum barrier height, U_b . Two separate methods for this comparison were investigated. The first method, similar to the 2-D simulation, employed an absolute energy limit: if $U^* \leq U_b$, placement of the particle was accepted, all else rejected. In the second method, particles were accepted if $U^* \leq U_b$ as before, but if $U^* > U_b$, placements were accepted with a probability $P = \min \{ \exp(-\Delta U), 1 \}$, where $\Delta U = U^* - U_b$. In view of the kinetic effects that are intended to be captured in the 3-D RSA algorithm, the second method, with $U_b = 0$, is most consistent with the usual stability ratio arguments of colloidal systems (20).

4. RESULTS AND DISCUSSION

We first present the effect of electrostatic interactions on both the fractional coverage and the structure of adsorbed

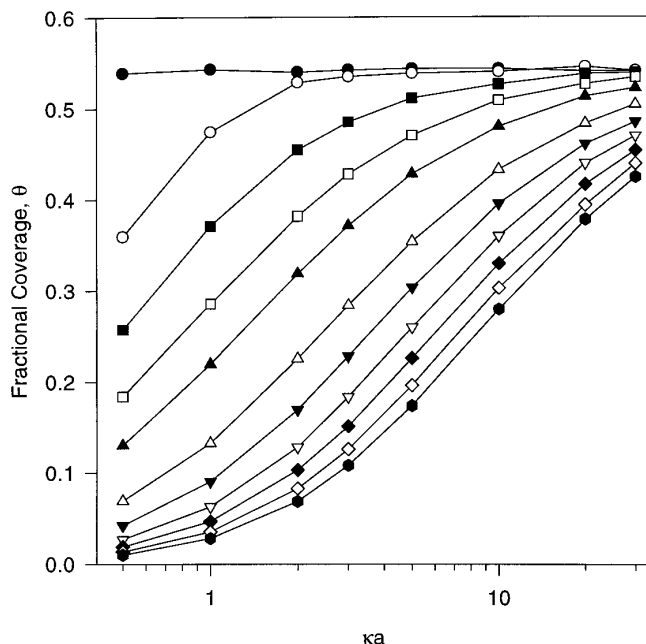


FIG. 5. 2-D RSA simulation results for $U_c = 1$. Each line connects points with constant values of B_{pp} : 0.3, \bullet ; 0.6, \circ ; 1.0, \blacksquare ; 1.7, \square ; 3.0, \blacktriangle ; 10, \triangle ; 30, \blacktriangledown ; 100, ∇ ; 300, \blacklozenge ; 1000, \diamond ; 3000, \bullet .

particles through an extensive 2-D RSA study and then explore the scaling behavior obeyed by both. A parametric study using the 3-D RSA model was not undertaken because thorough exploration of the model parameters is computationally prohibitive. Instead, we consider the 3-D RSA model with parameters approximating those for an experimental system (15) only. We compare the results of both 2-D and 3-D RSA simulations with experiment and then investigate the relationship between the two models. Finally, we discuss briefly the kinetics of adsorption.

4.1. General Results: 2-D RSA

The effect of electrolyte concentration. Two physical parameters control lateral repulsion between particles on the surface (see Eq. [8]): the Debye parameter, κ , which is proportional to the square root of the salt concentration, and B_{pp} , the characteristic electrostatic energy between particles. 2-D RSA simulations were carried out to explore the κa , B_{pp} dimensionless parameter space for various values of U_c (scaled by kT). The results for $U_c = 1$ are shown in Fig. 5. Each point represents the average of eight runs, and a different random number sequence was used for each run of 10 million placement attempts. The total surface area for placement was chosen to allow for approximately 1000 successful placements for each κa , B_{pp} pair. The ratio of the total surface area to the cross-sectional area of one particle therefore ranged from 2000 to 10,000.

The lines in each figure connect jamming limit fractional coverages for simulations at constant values of B_{pp} . Small

values of B_{pp} have little effect on the jamming limit coverage at any κa , and the jamming limit coverage matches that for hard disks, $\theta_{hd} \approx 0.55$. Under these conditions, the magnitude of electrostatic repulsion is small, so that U_{lat} never approaches U_c , and adsorption proceeds as if the particles were hard disks.

For larger values of B_{pp} , electrostatic repulsion between adsorbates becomes comparable to U_c , so fewer particles will fit on the surface. In this region of B_{pp} , the screening effect of the electrolyte becomes apparent. At low values of κa , the repulsion between particles is quite strong, and favorable adsorption occurs only at large interparticle separation distances. Regions within the configuration of adsorbed particles become inaccessible to adsorbing particles because of strong interparticle repulsion, and the fractional coverage is less than that for hard disks. Thus each particle can be considered to have an effective size greater than its actual size. Increased electrolyte concentration screens the electrostatic repulsion between particles, allowing for more closely packed configurations on the surface, and thus higher surface coverages. Thus as κa increases, θ_{max} asymptotically approaches the hard-disk limit.

Variation of the critical energy leads to systematic differences in adsorption behavior. An increase in U_c denotes an increase in the tolerance for interparticle repulsion, so that particles with a given B_{pp} at a fixed κa can pack more closely. As the value of U_c is increased, deviation from the hard-sphere jamming limit begins to occur at larger values of B_{pp} . Figure 6 shows a direct comparison of simulation results

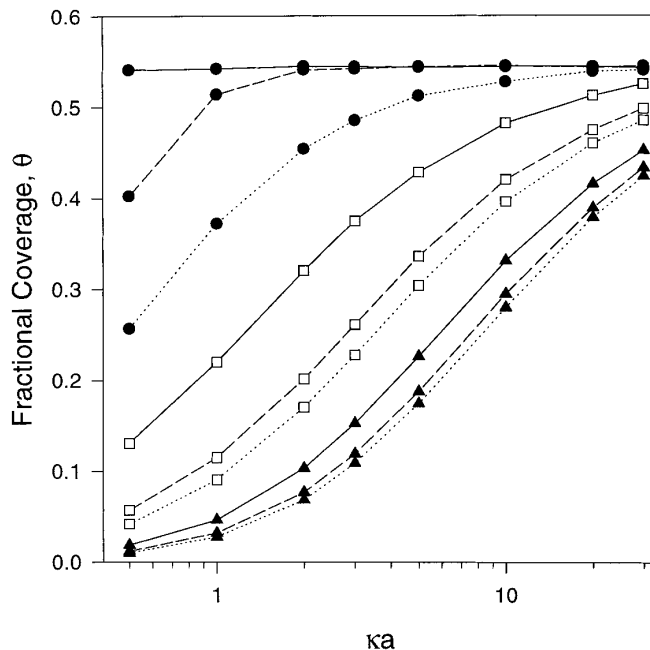


FIG. 6. 2-D RSA simulations for three different values of U_c . $U_c = 10$, solid line; $U_c = 2$, dashed line; $U_c = 1$, dotted line. $B_{pp} = 1$, \bullet ; $B_{pp} = 30$, \square ; $B_{pp} = 3000$, \blacktriangle .

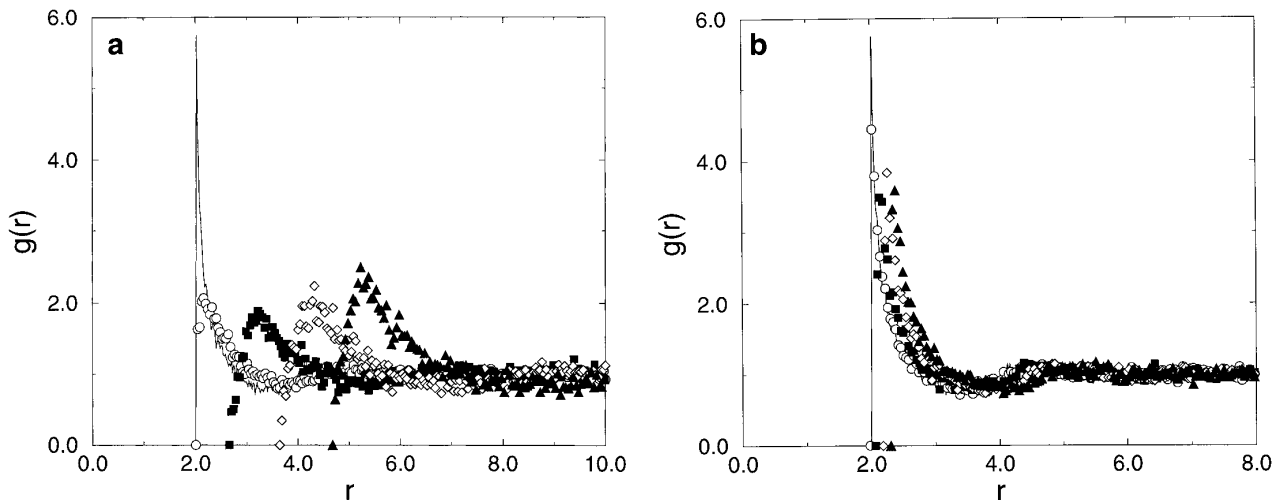


FIG. 7. Radial distribution functions from 2-D RSA simulations for (a) $\kappa a = 2$ and (b) $\kappa a = 20$. $U_c = 1$. B_{pp} values shown: 1.0, \circ ; 10, \blacksquare ; 100, \diamond ; 1000, \blacktriangle . The hard-disk RDF is given by the solid line.

($B_{pp} = 1, 30$, and 3000) for $U_c = 1, 2$, and 10 . The RSA simulations with low B_{pp} values are extremely sensitive to the choice of U_c : for $B_{pp} = 1$, substantial electrostatic repulsion is predicted for $\kappa a < 20$ when $U_c = 1$. However, hard-disk behavior is predicted when $U_c = 10$ over the same range of κa . In contrast, the adsorption characteristics for $B_{pp} = 30$ and 3000 are similar for the three values of U_c : electrostatic repulsion leads to a reduction in coverage as κa decreases. Figure 6 shows that simulation results are much less sensitive to U_c when $B_{pp} \gg U_c$, i.e., when repulsion is strong, the predicted limit varies little with U_c . This is presumably due to the exponential dependence of U_{pp}^{dl} on r in Eq. [8].

The study of B_{pp} , κa space clearly shows the limitations of the 2-D RSA model. The very large changes in θ_{max} seen in Fig. 5 for small B_{pp} at low κa are artifacts that appear when $B_{pp} \approx U_c$. The model is best suited to situations where interparticle repulsion is strong, where, in addition, the stability of the bulk suspension is assured. Thus, the RSA models in this work are inappropriate for the adsorption of small globular proteins, for which typically $B_{pp} \sim 1$ and $\kappa a \sim 1$. A further complicating factor for systems in the region of low B_{pp} is that the magnitude of the electrostatic interactions may approach that of van der Waals interactions, and the combination of the two may give rise to a more complex relationship between θ_{max} and electrolyte concentration.

The structural properties of the end-of-run configurations provide insight into the exclusion of particles by Yukawa repulsion. The radial distribution function (RDF), $g(r)$, details the average local density for a given configuration of particles (1, 25, 26). Selected RDFs are shown in Figs. 7a and 7b for $\kappa a = 2$ and $\kappa a = 20$, respectively, each with $U_c = 1$. Each RDF curve represents the average based on eight different configurations at the given values of B_{pp} and κa . For hard particles, $g(r)$ first takes on nonzero values when

$r = 2$ (27). In Fig. 7a, the position of the peak shifts to $r > 2$, and both the peak height and peak location gradually increase as B_{pp} increases. The shift in the location of the peak is evidence that the particle spacing is increasing, and as expected, this increase is related to the strength of the interparticle repulsion. When κa is increased, the added electrolyte screens repulsive electrostatic interactions—Fig. 7b shows that the RDF curves are not drastically different from that of hard disks. For $\kappa a = 20$, an increase in B_{pp} causes only a slight decrease in the peak height and a modest increase in peak position.

Scaling. For these Yukawa particles, $g(r)$ first becomes nonzero at separations $r \geq 2$, depending upon B_{pp} , κa , and U_c : electrostatic repulsion between particles renders some separation distances inaccessible. The exclusion of particles by Yukawa repulsion parallels excluded area effects in hard-particle RSA—each particle excludes an area that is approximately a circle of radius a' such that a'/a is one-half the average nearest-neighbor dimensionless separation distance. a'/a can be estimated for a given U_c by solving the Yukawa equation

$$U_c = \bar{N} \frac{B_{pp}}{2(a'/a)} e^{-2\kappa a[(a'/a)-1]}, \quad [18]$$

where \bar{N} is the average number of nearest neighbors. The number of nearest neighbors is usually estimated from the RDF of the jamming limit configuration (7),

$$\bar{N} = \int_0^{r_i} \frac{\theta_{max}}{\pi} g(r) 2\pi r dr, \quad [19]$$

where θ_{max} is the jamming-limit fractional coverage of “soft-disk” RSA of Yukawa-type particles, and r_i is the radial

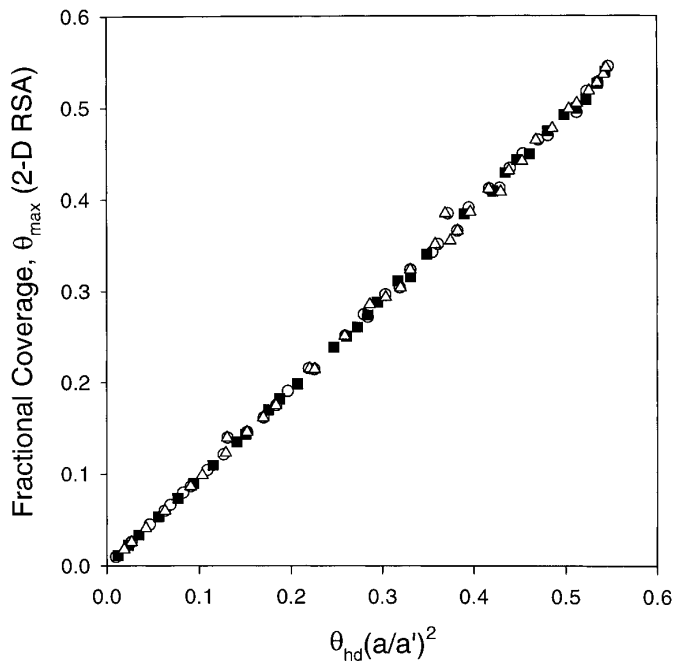


FIG. 8. Equation [20] plotted against θ_{\max} for various values of B_{pp} , κa . $U_c = 1$, \circ ; $U_c = 2$, \blacksquare ; and $U_c = 10$, \triangle .

position of the first trough in the RDF. Typically, for these systems, $\bar{N} \approx 6$. However, \bar{N} calculated in this way gives the average number of nearest neighbors in the *final* configuration, not the number of nearest neighbors present as each particle is placed. Integration to r_t also neglects energetic contributions from next-nearest neighbors, which may influence particle placement especially at low κa .

The calculation of Eq. [14] and the subsequent comparison of U_{lat} to U_c depends upon the local surface coverage, which is a function of time. As a consequence, the average energy per particle calculated from the final configuration is usually greater than U_c . Thus we consider \bar{N} in Eq. [18] to be an adjustable parameter, in the range of one to six. Once a' has been determined, RSA deposition of Yukawa particles should become a simple scaling of hard-disk RSA,

$$\theta_{\max} = \theta_{\text{hd}} \left(\frac{a}{a'} \right)^2, \quad [20]$$

where $\theta_{\text{hd}} = 0.547$. Equations [18] and [20] were fitted to the simulation results, θ_{\max} , for the corresponding values of B_{pp} , κa , and U_c ; a comparison is shown, in the form of Eq. [20], in Fig. 8. The value $\bar{N} = 3.5$ used there provided an excellent fit to the simulation results for the values of U_c studied.

Adamczyk *et al.* (1) presented an equation similar in form to Eq. [20], and the predictions of the two equations are compared in Fig. 9 for the values of U_c studied. The increase in coverage with U_c has been discussed above; the predic-

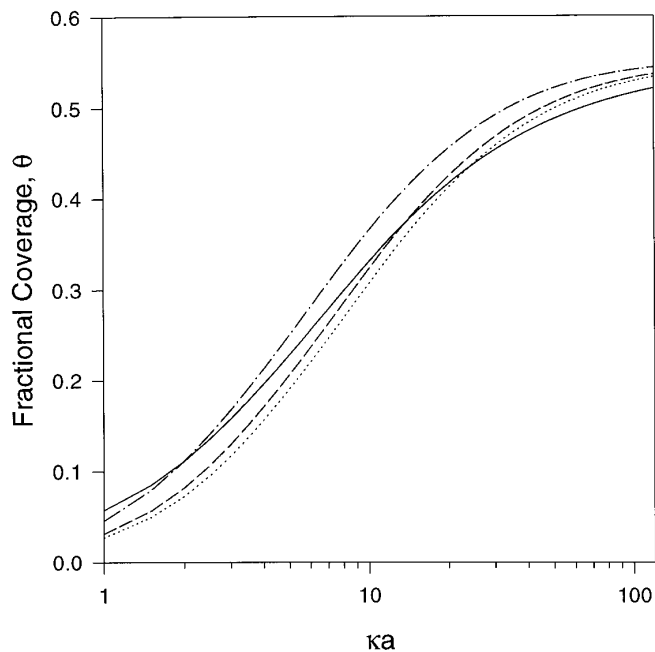


FIG. 9. Comparison between Eq. [20] (this work) and Eq. [20] of Adamczyk *et al.* (1). Adamczyk *et al.*, (—); Eq. [20] with $U_c = 1$, (\cdots); Eq. [20] with $U_c = 2$, (---); Eq. [20] with $U_c = 10$ (- \cdot - \cdot).

tions of Adamczyk *et al.* (who used $\bar{\phi}_0 = B_{pp} = 200$), fall within the range of our predictions.

The formulation in Eq. [18] also allows scaling of the RDF. When RDFs for a given κa are rescaled from r to $r' = R/a'$, all curves for which $a'/a > 1$ collapse onto a single curve. Figure 10 shows rescaled RDF curves for κa of 2

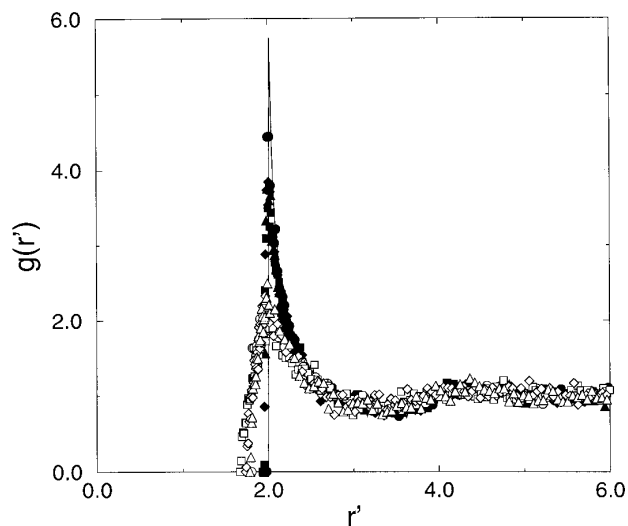


FIG. 10. Radial distribution functions from Fig. 7 for $\kappa a = 2$ and 20, rescaled by $r' = R/a'$. Open symbols correspond to $\kappa a = 2$ and filled symbols correspond to $\kappa a = 20$. Circles, squares, diamonds, and triangles for both κa values correspond to $B_{pp} = 1, 10, 100$, and 1000, respectively. The number of points was reduced for clarity. The hard-disk RDF is given by the solid line.

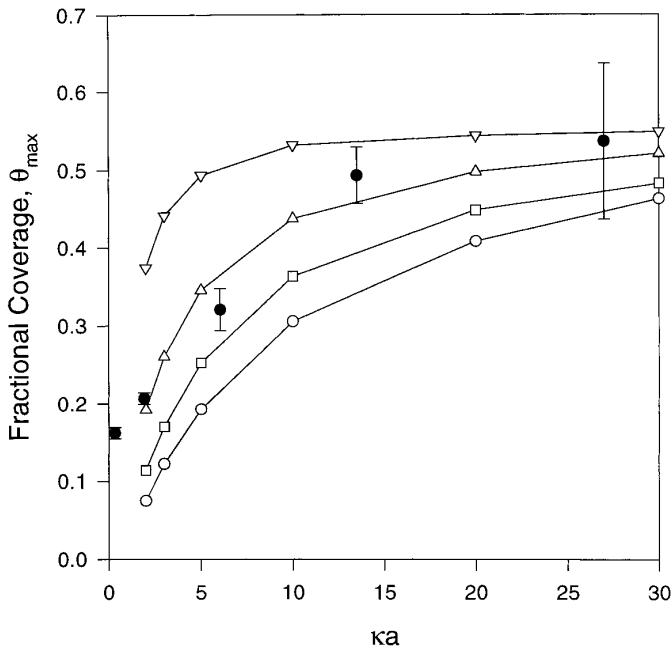


FIG. 11. Comparison of 2-D RSA simulation of amidine polystyrene adsorption with the experimental AFM results of Johnson and Lenhoff (15). AFM data, \bullet ; $U_c = 1$, \circ ; $U_c = 10$, \square ; $U_c = 100$, \triangle , ∇ .

(open symbols) and 20 (filled symbols). The rescaled RDF for $\kappa a = 2$ is representative of the behavior at low κa : the peak height of the single curve falls well below that of the hard-disk RDF. In addition, the scaled RDF curve begins slightly below $r' = 2$. This is likely to be a result of the approximate estimation of a' , and is a manifestation of the softness of the Yukawa particles. At high κa , the scaled RDF matches the hard-disk RDF quite closely.

4.2. Comparison with Experiment

The 2-D RSA simulation was used to model the adsorption of the amidine polystyrene latex particles for which experimental results have been reported previously (15). The simulation results are shown in Fig. 11 for $U_c = 1, 10, 100,$ and 1000 along with experimentally determined surface coverages. Each point represents the average of three independent simulation runs. The simulation captures the experimentally observed trend, namely, the fractional coverage increases as electrolyte concentration increases. Additional electrolyte weakens repulsion between particles both directly, through screening effects (Eq. [8]), and indirectly, through the reduction in B_{pp} , the characteristic repulsion between particles (Eq. [9]). B_{pp} values were calculated using Eq. [9] with $a = 58$ nm and $\sigma_s = 27.4$ mC/m², and ranged from 1700 ($\kappa a = 2$) to 150 ($\kappa a = 30$). From Fig. 11 it is apparent that the simulation results for $U_c = 100$ provide a good fit to the experimental data. Polydispersity of size and surface charge density of the latex particles may obfuscate

the comparison between simulation results and experimental data. If U_c represents the tradeoff between unfavorable particle repulsion and favorable particle-surface interaction energy, one would estimate the critical energy to be $U_c \sim 1000$ (Table 1). We conclude that U_c has little connection to the energy of adsorption within the context of this simple 2-D RSA model, but serves as a useful adjustable parameter. In the next section, we study the relationship between U_c and the more physically appealing U_b of the 3-D RSA model.

Instead of an exhaustive exploration of the $B_{pp}, B_{ps}, \kappa a$ parameter space for the 3-D RSA algorithm, we restricted our study to the model parameters of the polystyrene latex-mica system. Fractional coverage versus κa for the simulated latex-mica system is shown in Fig. 12a for $U_b = 1, 2,$ and 10 for the absolute acceptance method. Results of the 3-D simulation for the probabilistic acceptance method are shown in Fig. 12b for $U_b = 0, 1, 2,$ and 10 . Each point represents an average of 10 runs of 10 million placement attempts, with a different random number sequence used for each run. The ratio of total surface area for placement to the cross-sectional area of one particle ranged from 2300 to 6600 so that each simulation would yield at least 1000 successful placements.

Both 3-D simulations yield trends in salt-dependent adsorption similar to that observed experimentally. The agreement between the model and the data is good for both acceptance methods, and the agreement improves slightly as U_b approaches 10. The fractional coverages in the 3-D RSA with probabilistic acceptance are higher than the coverages of the corresponding 3-D simulations with absolute acceptance. This occurs because values of U^* greater than U_b can still lead to successful placement with the probabilistic acceptance criterion. Figures 12a and 12b show that the results for both models are not very sensitive to the choice of U_b , and this may be attributed to the large difference between U_b and B_{ps} . U_b represents the maximum surmountable energy barrier to adsorption, so values of $O(1)$ are reasonable choices for this model parameter. Given the inherent nonidealities of the experimental system and the approximations in calculating interaction energies U_{pp} and U_{ps} , $U_b = 10$ is not an unreasonably large estimate.

4.3. Relationship between 2-D RSA and 3-D RSA

Both 2-D and 3-D RSA simulations capture the behavior of θ_{max} with salt concentration reasonably well, each with the aid of one adjustable parameter. The physical interpretation of these parameters clearly depends upon the model construct. In the 2-D model, U_c specifies the particular value of the interaction energy between particles at the surface, U_{lat} , above which adsorption is too energetically expensive. U_b , used in the 3-D model, fixes the maximum amount of kinetic energy available to particles to overcome the energetic barrier to adsorption, U^* . The purpose of this section is to study the relationship between U_{lat} and U^* .

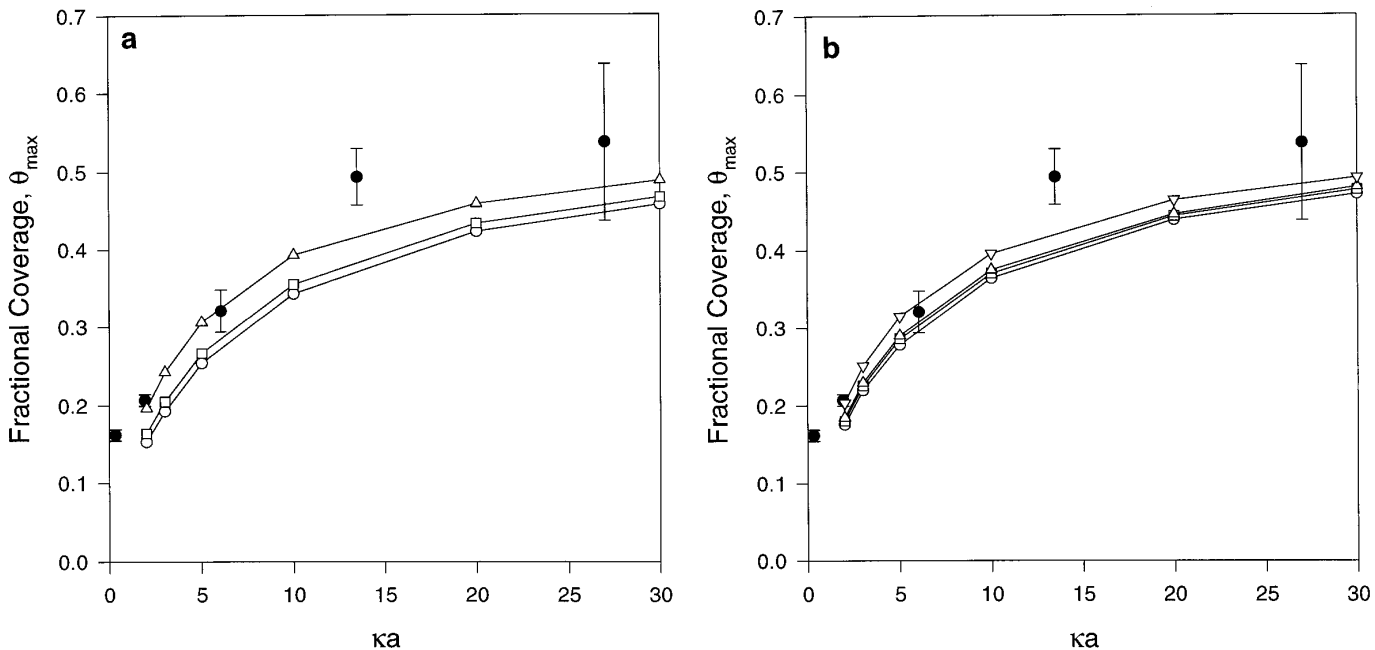


FIG. 12. Comparison of 3-D RSA simulation of amidine polystyrene adsorption with the experimental AFM results of Johnson and Lenhoff (15). In (a), the absolute acceptance criterion was used: AFM data, \bullet ; $U_b = 1$, \circ ; $U_b = 2$, \square ; $U_b = 10$, \triangle . In (b), the probabilistic acceptance criterion was used: AFM data, \bullet ; $U_b = 0$, \circ ; $U_b = 1$, \square ; $U_b = 2$, \triangle ; $U_b = 10$, ∇ .

While both U_{lat} and U^* depend upon the local surface concentration, only U^* depends upon the physical properties of the surface–particle interaction. To study the relationship between the two, the values of U^* were calculated for the placement of a particle at various positions on the surface near to one adsorbed particle, or at a position equidistant from two, three, or four adsorbed particles. The value of U_{lat} for each configuration was also calculated. Figures 13a and 13b show the relationship between U_{lat} and U^* for $\kappa a = 19$ and $\kappa a = 1.9$, respectively. For both cases, U_{lat} is substantially larger than U^* for a given configuration of adsorbates, and so U_c overestimates the kinetic barrier. However, in the $\kappa a = 19$ case there is a good correlation between U_{lat} and U^* , so one could still use the simpler 2-D RSA model with the appropriate correction to U_c . For example, setting $U_c = 2.5$ in the 2-D simulation should correspond to an actual barrier height of approximately $U_b = 1$ in the 3-D simulation.

Figure 14 shows that the average RDF of a 2-D RSA simulation with $U_c = 2.5$ very nearly coincides with that of the corresponding 3-D RSA simulation with $U_b = 1$ (absolute acceptance) at $\kappa a = 20$. For the $\kappa a = 1.9$ case, the relationship between U_{lat} and U^* exhibits a more complex dependence upon the configuration. From Fig. 13b, it appears that a 2-D simulation with $U_c = 50$ should match the 3-D RSA results more closely. Figure 14 shows a comparison between radial distribution functions of the 2-D and 3-D simulations (with absolute acceptance) for $\kappa a = 2$. The structure of the 2-D simulation with $U_c = 50$ provides a much closer match to that of the 3-D simulation with $U_b =$

1, as expected. The RDF curves for both 2-D RSA simulations begin at larger values of r as compared to the 3-D simulation, which is consistent with the lower fractional coverages obtained.

4.4. Adsorption Kinetics

As a consequence of the finite nature of computer simulations, the jamming limit fractional coverage for RSA simulations is usually determined by extrapolation (1, 11). However, the extrapolation procedure appears to have limited applicability for both the 2-D and 3-D RSA of Yukawa particles.

The number of placement attempts required to reach the jamming limit depends upon the ratio of the particle radius a to the length of the square simulation box L . Adamczyk *et al.* (1) defined a pseudo-time variable τ as the ratio $\tau = N_{\text{att}}/N_{\text{ch}}$, where N_{att} is the actual number of placement attempts and $N_{\text{ch}} = 0.547L^2/\pi a^2$ is the characteristic number of placement attempts. At large values of τ for hard disks, the relationship between the fractional coverage $\theta(\tau)$ and the jamming limit fractional coverage $\theta(\tau \rightarrow \infty)$ is (11, 28)

$$\theta(\infty) - \theta(\tau) \sim \tau^{-1/2}. \quad [21]$$

By plotting $\theta(\tau)$ versus $1/\sqrt{\tau}$ for $\tau > 1$ and extrapolating linearly as $1/\sqrt{\tau} \rightarrow 0$ (i.e., $N_{\text{att}} \rightarrow \infty$), the intercept obtained is the jamming limit, θ_{\max} .

Figure 15 shows this analysis for one 2-D RSA run and

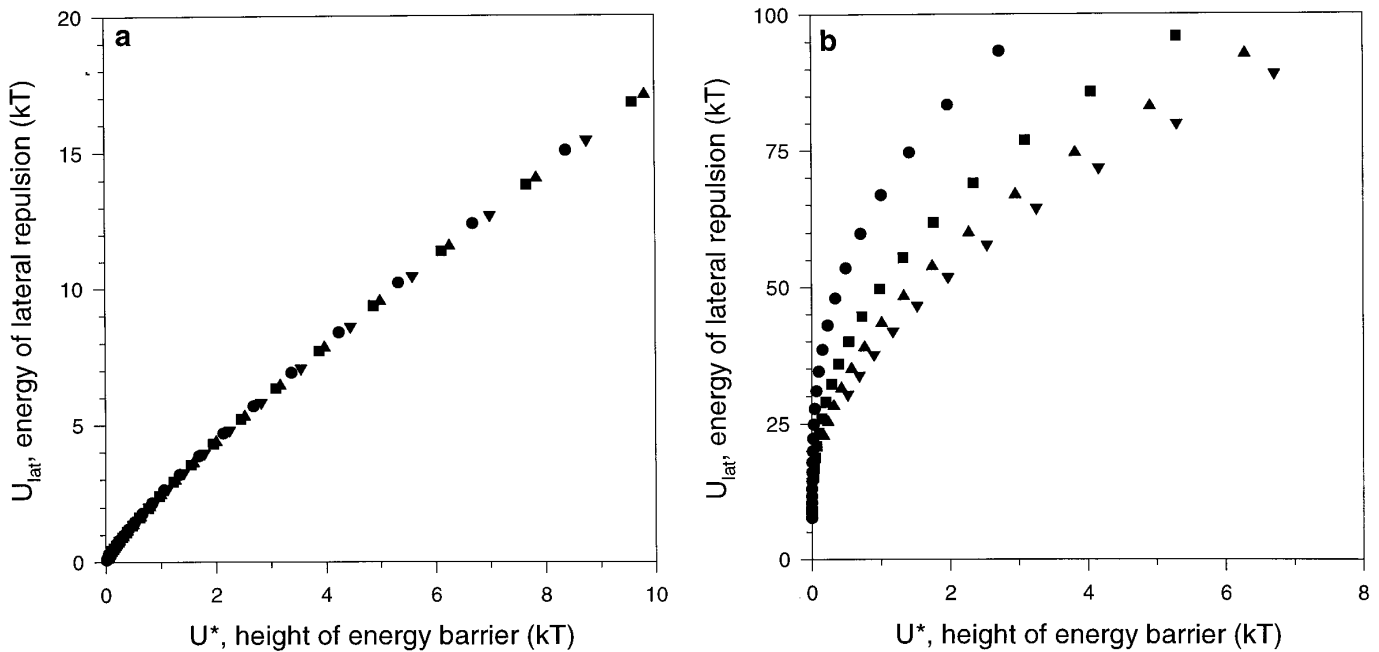


FIG. 13. Comparison of U_{lat} with U^* for amidine polystyrene latex particles. (a) $\kappa a = 19$ and (b) $\kappa a = 1.9$, with energies calculated for configurations with $N = 1$, \bullet ; $N = 2$, \blacksquare ; $N = 3$, \blacktriangle ; and $N = 4$, \blacktriangledown .

two 3-D RSA runs, each at $\kappa a = 5$. For the 2-D RSA run (circles), $B_{\text{pp}} = 10$ and $U_c = 1$; this run is representative of all 2-D RSA runs. One of the 3-D RSA runs (diamonds) was performed with the absolute acceptance method while the other (squares) was performed with probabilistic acceptance. For both 3-D RSA runs, $U_b = 1$, and the pair is representative of all 3-D RSA runs. The solid lines are the linear best fit to the simulation data for $\tau^{-1/2} \leq 1$.

The adsorption kinetics for the 2-D RSA and the 3-D RSA with absolute acceptance follow Eq. [21] except at very long times, when the fractional coverage begins to level off to a region of zero slope. Extrapolation from the linear region (nonzero slope) would yield a jamming limit coverage higher than that attainable for given energy requirements. Thus, fractional coverages shown in this work are not extrapolated values, but end-of-run values from the plateau region.

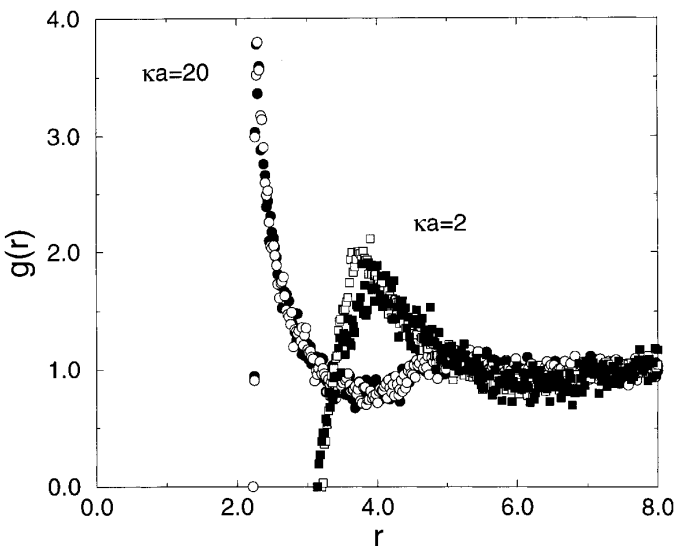


FIG. 14. Radial distribution functions of 2-D RSA and 3-D RSA simulations (with absolute acceptance) of polystyrene latex particles for $\kappa a = 2$ and 20. For $\kappa a = 2$, $U_c = 50$ for the 2-D simulation (\square) and $U_b = 1$ for the 3-D simulation (\blacksquare). For $\kappa a = 20$, $U_c = 2.5$ (\circ), and $U_b = 1$ (\bullet).

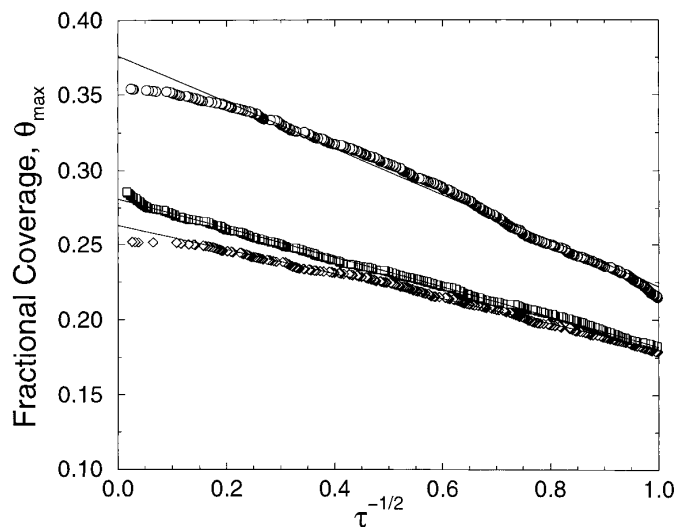


FIG. 15. Kinetic analysis of 2-D and 3-D RSA adsorption using Eq. [21]. For all three runs, $\kappa a = 5$. 2-D RSA with $B_{\text{pp}} = 10$ and $U_c = 1$, \circ ; 3-D RSA with probabilistic acceptance, $U_b = 1$, \square ; 3-D RSA with absolute acceptance, $U_b = 1$, \diamond . Solid lines indicate linear least-squares fit of the data over the range $\tau^{-1/2} \leq 1$.

The kinetics for probabilistic acceptance method in the 3-D RSA model show a positive deviation from Eq. [21] at very long times. The positive deviations occur despite energetic considerations because the acceptance is probabilistic: placements for which $U^* > U_b$ still have a small but finite probability of acceptance. Consequently, Fig. 15 suggests that, given sufficient simulation time, RSA simulations with a probabilistic acceptance criterion would show no dependence upon κa .

5. CONCLUSIONS

We have developed two random sequential adsorption techniques to model the adsorption characteristics of charged colloidal particles in electrolyte solutions. The 2-D RSA simulation does not differ greatly from that of Adamczyk *et al.* (1) in the estimation of fractional coverages, despite two key differences: (1) the energy of interaction U_{lat} was calculated by consideration of many neighbors, not just the nearest; and (2) acceptance of placement attempts was based on direct comparison with a fixed adjustable parameter, U_c , rather than on the probabilistic criterion. The 2-D RSA parametric study of κa , B_{pp} space led to a simple method of estimating surface coverage for a given salt concentration. The correlation of fractional coverage with effective radius, though still approximate, was developed by consideration of the time-dependent configurational properties of the system.

Model parameters calculated for amidine polystyrene latex beads were used in the 2-D RSA model and the simulation results were compared with experimental data for the adsorption of these particles onto mica. While 2-D RSA captures the observed increase of fractional coverage with the increase of electrolyte concentration, the value of the only adjustable parameter used, U_c , that produced the best fit did not have a physically meaningful interpretation. The 2-D RSA model is not suitable for modeling the adsorption of colloids such as globular proteins, for which electrostatic repulsion is too weak.

The 3-D RSA simulation, developed with the use of a three-body superposition approximation, provides a more realistic depiction of adsorption physics. Direct calculation of the particle–surface attractive interaction energy along with the particle–particle repulsion can give rise to a kinetic barrier to adsorption. One adjustable parameter, U_b , was used in this model to characterize the maximum surmountable barrier height. However, because its value was small compared to the characteristic electrostatic repulsion energy studied, the simulation predictions were fairly insensitive to the physically meaningful values of this parameter. Simulation results match experimental data (15) quite well, except at high κa , where experimental uncertainty is thought to contribute to the discrepancy.

Thus the 3-D RSA simulation captures more realistically the physical events that occur during adsorption, but at in-

creased computational expense. The 2-D RSA simulation provides a simple prediction of fractional coverage with one nonphysical parameter.

APPENDIX

Superposition Approximation for Two Interacting Spheres

In this Appendix, we give a sketch of the origin of the expressions in Eqs. [8] and [9]. It is easier to use dimensional quantities.

The key idea of the superposition approximation for fairly widely separated spheres is due to Bell *et al.* (29). A long distance R from a single particle of radius a (that is, with $\kappa R \gg 1$) the electrostatic potential ψ satisfies

$$\psi \sim Y \frac{a}{R} e^{-\kappa(R-a)} \quad [22]$$

for some constant Y , the effective surface potential. (In the Debye–Hückel approximation, Y is equal to the surface potential of the sphere ψ_p .)

The superposition approximation says that, when two particles of radii a_1 and a_2 and effective potentials Y_1 and Y_2 interact with smallest separation $h \gg 1/\kappa$, the potential is well-approximated by summing the potentials surrounding each sphere in isolation. By integrating the stress tensor over the midplane between the spheres, the force can be calculated. Then integrating force with respect to separation h gives the interaction free energy:

$$F^{\text{dl}} = 4\pi\epsilon_0 Y_1 Y_2 \frac{a_1 a_2}{(a_1 + a_2 + h)} e^{-\kappa h}. \quad [23]$$

In the nonlinear case we need expressions for Y_1 and Y_2 in terms of ψ_p and κa .

Chew and Sen (18) obtained a matched asymptotic expansion for the potential ψ a distance s from the center of a sphere, radius a , surface potential ψ_p . This expansion has error of order $1/(\kappa a)^2$.

At large distances from the surface (when $x \equiv \kappa(R - a) \gg 1$) the potential has the form

$$\psi_0 = \frac{kT}{e} \left\{ 4\gamma + \frac{2}{\kappa a} \gamma^3 \right\} \frac{a}{R} e^{-x}, \quad [24]$$

where $\gamma = \tanh[e\psi_p/(4kT)]$. It is this outer expansion that provides an expression for Y_1 and Y_2 . Substituting this into Eq. [23] and converting to scaled variables produces Eqs. [8] and [9].

When $a_2 = \infty$ (a flat surface), we have

$$F^{\text{dl}} = 4\pi\epsilon_0 Y_1 Y_2 a_1 e^{-\kappa h}, \quad [25]$$

where Y_2 contains only the first term since there are now no corrections involving κa . Hence one gets Eqs. [15] and [16].

Close to the surface (when $x = O(1)$) the potential is

$$\psi_1 = \frac{kT}{e} \left\{ 2 \log \left[\frac{1 + \gamma e^{-x}}{1 - \gamma e^{-x}} \right] + \frac{2}{\kappa a} \frac{\gamma e^{-x} [\gamma^2 (1 - e^{-2x}) - 2x]}{1 - \gamma^2 e^{-2x}} \right\}. \quad [26]$$

If the surface charge density σ_p of the sphere is held constant, then the relationship between σ_p and ψ_p is

$$\sigma_p = \epsilon \epsilon_0 \kappa \frac{kT}{e} \left\{ 2 \sinh \frac{e\psi_p}{2kT} + \frac{4}{\kappa a} \tanh \frac{e\psi_p}{4kT} \right\}, \quad [27]$$

which comes from differentiating the inner expansion and evaluating at the surface. Equation [27] is accurate to within 5% for all values of ψ_s when $\kappa a > 0.5$.

Matching [24] and [26] for intermediate values of x yields the uniform expansion

$$\psi = \psi_0 + \psi_1 - \frac{kT}{e} \left\{ 4\gamma e^{-x} + \frac{2}{\kappa a} \gamma(\gamma^2 - 2x)e^{-x} \right\}, \quad [28]$$

which was the main result in (18).

ACKNOWLEDGMENTS

D.Y.C., S.L.C., and J.S. gratefully acknowledge partial support for this work from the Advanced Minerals Product Centre, a Special Research Centre Funded by the Department of Employment, Education and Youth Affairs of the Australian Federal Government. A.M.L. and M.R.O. gratefully acknowledge the support of the National Science Foundation (Grant CTS-9321318), as well as the hospitality of the Advanced Mineral Products Centre. M.R.O. thanks Dr. John Elie Sader for many helpful discussions.

REFERENCES

- Adamczyk, Z., Zembala, M., Siwek, B., and Warszynski, P., *J. Colloid Interface Sci.* **140**, 123 (1990).
- Nicholson, D., and Parsonage, N. G., "Computer Simulation and the Statistical Mechanics of Adsorption." Academic Press, New York, 1982.
- Vernov, A. V., and Steele, W. A., *Langmuir* **2**, 219 (1986).
- Haynes, C. A., and Norde, W., *Colloids Surf. B* **2**, 517 (1994).
- Chatelier, R. C., and Minton, A. P., *Biophys. J.* **71**, 2367 (1996).
- Ross, S., and Oliver, J. P., "On Physical Adsorption." Interscience, New York, 1964.
- Löwen, H., *J. Phys. Condens. Matter* **4**, 10105 (1992).
- Ansell, G. C., and Dickinson, E., *Chem. Phys. Lett.* **122**, 594 (1985).
- Oberholzer, M. R., Wagner, N. J., and Lenhoff, A. M., *J. Chem. Phys.*, in press (1997).
- Johnson, C. A., Wu, P., and Lenhoff, A. M., *Langmuir* **10**, 3705 (1994).
- Feder, J., *J. Theor. Bio.* **87**, 237 (1980).
- Feder, J., and Giaever, I., *J. Colloid Interface Sci.* **78**, 144 (1980).
- Schaaf, P., and Talbot, J., *Phys. Rev. Lett.* **62**, 175 (1989).
- Tarjus, G., Schaaf, P., and Talbot, J., *J. Chem. Phys.* **93**, 8352 (1990).
- Johnson, C. A., and Lenhoff, A. M., *J. Colloid Interface Sci.* **179**, 587 (1996).
- Carnie, S. L., Chan, D. Y. C., and Stankovich, J., *J. Colloid Interface Sci.* **165**, 116 (1994).
- Stankovich, J., and Carnie, S. L., *Langmuir* **12**, 1453 (1996).
- Chew, W. C., and Sen, P. N., *J. Chem. Phys.* **77**, 2042 (1982).
- O'Brien, R. W., and White, L. R., *J. Chem. Soc. Faraday II* **74**, 1607 (1978).
- Hunter, R. J., "Foundations of Colloid Science," Vol. 1. Oxford Univ. Press, Oxford, 1987.
- Carnie, S. L., Chan, D. Y. C., and Gunning, J. S., *Langmuir* **10**, 2993 (1994).
- McCormack, D., Carnie, S. L., and Chan, D. Y. C., *J. Colloid Interface Sci.* **169**, 177 (1995).
- Adamczyk, Z., Zembala, M., Siwek, B., and Warszynski, P., *Adv. Colloid Interface Sci.* **48**, 151 (1994).
- Adamczyk, Z., and Waroński, P., *Langmuir* **11**, 4400 (1995).
- Allen, M. P., and Tildesley, D. J., "Computer Simulations of Liquids." Oxford Univ. Press, Oxford, UK, 1987.
- MacQuarrie, D. A., "Statistical Mechanics." Harper Collins, New York, 1976.
- Chae, D. G., Ree, F. H., and Ree, T., *J. Chem. Phys.* **50**, 1581 (1968).
- Swendsen, R. H., *Phys. Rev. A* **24**, 504 (1981).
- Bell, G. M., Levine, S., and McCartney, L. N., *J. Colloid Interface Sci.* **33**, 335 (1970).